ELSEVIER

Earth and Planetary Science Letters 184 (2001) 605–621

EPSL

www.elsevier.com/locate/epsl

# The density structure of subcontinental lithosphere through time

Yvette H. Poudjom Djomani [a,*], Suzanne Y. O'Reilly [a], W.L. Griffin [a,b], P. Morgan [a]

[a] *GEMOC ARC National Key Centre, Department of Earth and Planetary Sciences, Macquarie University, Sydney, N.S.W. 2109, Australia*

[b] *CSIRO Exploration and Mining, P.O. Box 136, North Ryde, N.S.W. 1670, Australia*

Received 5 October 2000; accepted 23 November 2000

**Abstract**

This study uses information on composition, thermal state and petrological thickness to calculate the densities of different types of subcontinental lithospheric mantle (SCLM). Data from mantle-derived peridotite xenoliths and garnet–xenocryst suites document a secular evolution in the composition of SCLM: the mean composition of newly formed SCLM has become progressively less depleted, in terms of Al, Ca, mg# and Fe/Al, from Archean, through Proterozoic to Phanerozoic time. Thermobarometric analyses of xenolith and xenocryst suites worldwide show that the mean lithospheric palaeogeotherms rise from low values (corresponding to surface heat flows of 35–40 mW/m$^2$) beneath Archean terranes, to higher values ($>50$ mW/m$^2$) beneath regions with Phanerozoic crust. The typical thickness of the lithosphere (defined as a chemical boundary layer), ranges from about 250 to 180 km, 180–150 km and 140–60 km for Archean, Proterozoic and Phanerozoic terranes respectively. The depth of this lithosphere–asthenosphere boundary corresponds to a temperature of 1250–1300°C. Using the estimated compositions, average mineral compositions and experimental data on the densities of mineral end-members (tables 1 and 2), we calculate mean densities at 20°C for Primitive Mantle (3.39 Mg m$^{-3}$) and for SCLM of Archean ($3.31 \pm .016$ Mg m$^{-3}$), Proterozoic ($3.35 \pm 0.02$ Mg m$^{-3}$) and Phanerozoic ($3.36 \pm 0.02$ Mg m$^{-3}$) age. Curves of density and cumulative density versus depth, which take into account variations in geotherm with tectonothermal age, have been constructed for each age type of lithospheric section to assess the buoyancy of these columns relative to the asthenosphere, modelled as a Primitive Mantle composition. The density curves show that Archean SCLM is significantly buoyant relative to the asthenosphere at depths greater than about 60 km. Proterozoic sections deeper than about 100 km thick also are significantly buoyant. The buoyancy of Archean and Proterozoic SCLM sections, combined with their refractory composition, leads to high viscosities and explains the longevity and stability of old SCLM. Replacement of Archean lithosphere, as beneath the present-day eastern Sino–Korean craton, probably involves mechanical dispersal by rifting, accompanied by the rise of hot, fertile asthenospheric material. Fertile Phanerozoic lithosphere is buoyant when the geotherm is sufficiently high, as in many Cenozoic volcanic provinces. However, as the geothermal gradient relaxes toward a stable conductive profile, Phanerozoic SCLM sections thinner than about 100 km become denser than the asthenosphere, and hence gravitationally unstable. This could help to induce delamination of the SCLM and upwelling of asthenospheric material, beginning a new cycle. The tectonic consequences of such lithosphere replacement would include uplift and

* Corresponding author. Tel.: +61-2-9850-9673; Fax: +61-2-9850-8943; E-mail: ypoudjom@brunhes.es.mq.edu.au

0012-821X/01/$ – see front matter 
PII: S0012-821X(00)00362-9

magmatism, and basin formation during subsequent thermal relaxation. 

*Keywords:* lithosphere; composition; mantle; density; geothermal gradient; xenoliths

## 1. Introduction

The subcontinental lithospheric mantle (SCLM) carries a geochemical, thermal and chronological record of large-scale tectonic events that have shaped the Earth's crust. The SCLM is part of the continental plate, and moves with the plate over the weak asthenosphere. The idea that 'old' (cratonic) lithosphere is relatively thick, depleted and cold has been long accepted by petrologists ([1] and references therein). Recognition that 'young' lithosphere is relatively thin, fertile and hot is more recent; Jordan [2] observed that the thermal boundary layer (TBL) beneath late-Proterozoic and Phanerozoic mobile belts is more similar to oceanic mantle than to cratonic mantle in its geophysical characteristics.

Development of the 4-D Lithosphere Mapping methodology [1] has allowed the construction of realistic geological sections of the SCLM in a wide variety of tectonic settings and at different times. Xenoliths and garnet and chromite xenocrysts from mantle-derived volcanic rocks (e.g. basalts, lamproites, kimberlites) provide samples of the lithospheric mantle at the time of eruption. Where sufficient xenoliths and/or xenocrysts of appropriate composition are available, determination of the palaeogeotherm, the depth to the crust–mantle boundary, the detailed distribution of rock types with depth within the SCLM, and the depth to the petrological lithosphere–asthenosphere boundary (LAB) within the tectosphere is possible [1]. Mantle sections constructed in this way provide a basis for the calculation of physical properties (such as density) of specific lithosphere domains.

## 2. Palaeogeotherms and lithosphere thickness

### 2.1. Construction of palaeogeotherms

The distribution of temperature with depth at the time of a given volcanic eruption (the palaeogeotherm) is one of the key parameters that must be determined to derive the density of a column of SCLM. Empirical palaeogeotherms are derived by geothermobarometric calculations based on mineral chemistry, using methods with experimental or theoretical calibration relevant to the mineral assemblage, bulk composition and equilibration conditions of particular samples (e.g. [3,4]). Where xenoliths with mineral assemblages appropriate for calculation of both pressure and temperature of equilibration are available, several geothermobarometers commonly give concordant results for a xenolith suite, even though results from the application of different techniques to a single sample may show a high variance (e.g. [5,6]).

The limited geographic and temporal distribution of xenolith suites is a major problem in this approach, and in many suites (especially those from basalts) only a small number of xenoliths in a suite may have appropriate mineral assemblages. The situation has been improved by the development of single-element thermometers (Ni in garnet, Zn in chromite) based on partitioning between these phases with mantle olivine, and a methodology for derivation of geotherm parameters from suites of garnet and spinel xenocrysts [6]. Where suites of both xenoliths and xenocrysts are available, the two approaches give concordant results ([6,7]).

Surface heat-flow values and xenolith-derived mantle geotherms are commonly linked through assumptions such as those made in the downward extrapolation of temperature from surface heat flow by Pollack and Chapman [8]. However, these assumptions include poorly constrained models of

the distributions of thermal conductivity and radiogenic heat production with depth which are laterally variable. In general, surface heat flow is a function of both the geotherm at depth and upper crustal heat production, and the mantle geotherm and surface heat flow may be only weakly linked. In the Pollack and Chapman model [8], the mantle geotherm is directly linked to the surface heat flow by assuming that 60% of the surface heat flow is derived from below the upper crust. We use this model here to illustrate a rough global average surface heat flow equivalent to the mantle geotherms that we model, not an attempt to model any particular local geotherm. In most cratonic areas, and in Phanerozoic regions without active Neogene volcanism, palaeogeotherms derived from both xenoliths and xenocrysts tend to parallel theoretically constructed model conductive geotherms such as those of Pollack and Chapman [8]. These geotherms are strongly model-dependent, involving assumptions that include the distribution of heat production and thermal conductivity with depth and the variation of thermal conductivity with temperature. The same surface heat flow can result from a range of heat-production distributions, and similar lithospheric mantle geotherms may give rise to different surface heat flows, depending on the structure and composition of the crust (e.g. [9,10]). However, the model geotherms of Pollack and Chapman [8], which are parameterised in terms of the surface heat flow, provide a convenient reference frame for comparison of the xenolith and xenocryst data between different areas. We have constructed, or collected from the literature, xenolith/xenocryst-based palaeogeotherms for more than 300 localities worldwide, and classified these by their tectonothermal age (i.e. the age of the last major thermal event in the crust [1]). These empirically determined palaeogeotherms are typically low beneath Archean cratonic areas, higher beneath Proterozoic regions, and still higher beneath areas of Phanerozoic tectonic activity, corresponding broadly to global variations in surface heat flow ([9]; Fig. 1). Furthermore, the observed differences in lithospheric mantle temperature are

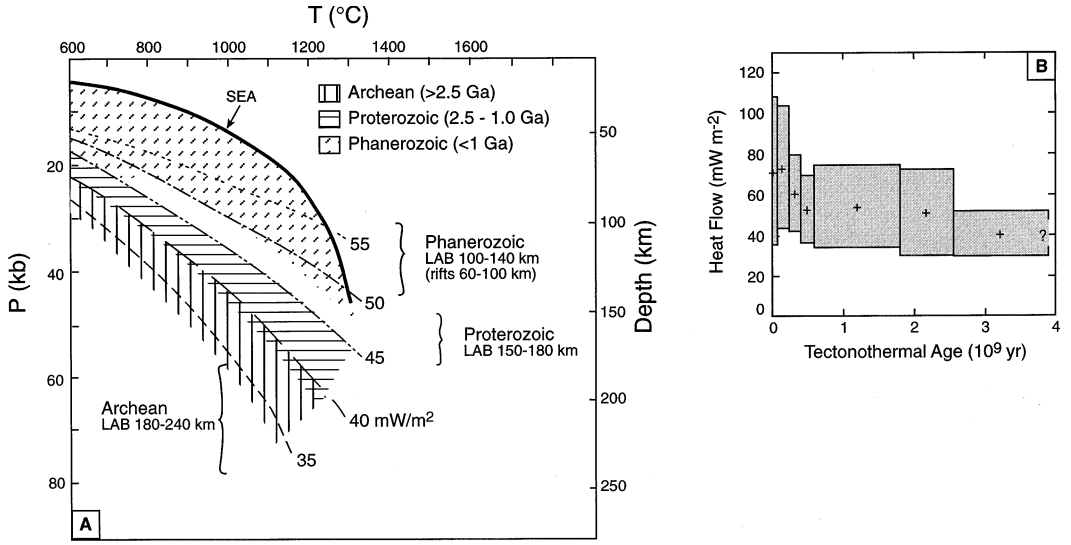


Fig. 1. (A) The range of $P$–$T$ conditions commonly derived from xenolith and xenocryst suites in volcanic rocks that penetrate crust of different tectonothermal age (crustal age domains modified from Janse [15]: Archean, $\geq$2.5 Ga; Proterozoic, 2.5–1.0 Ga; Phanerozoic, $<$1 Ga). Also shown is the range of depths to the LAB typical of each group, as defined by the maximum depth of $Y$-depleted garnets beneath Archean and Proterozoic cratons (Ryan et al. [6]), and the maximum depth of sampling in Phanerozoic regions. Reference geotherms are conductive models of Pollack and Chapman [8], labelled with corresponding surface heat flow in mW/m$^2$, and the southeastern Australia advective geotherm (SEA) derived from xenoliths in basalts [12]. (B) Variation of surface heat flow measurements with tectonothermal age of the crust (after Morgan [9]). The crosses at the centre of the boxes represent the mean heat flow for each age group; note the general correlation with the range of geotherms in (A).

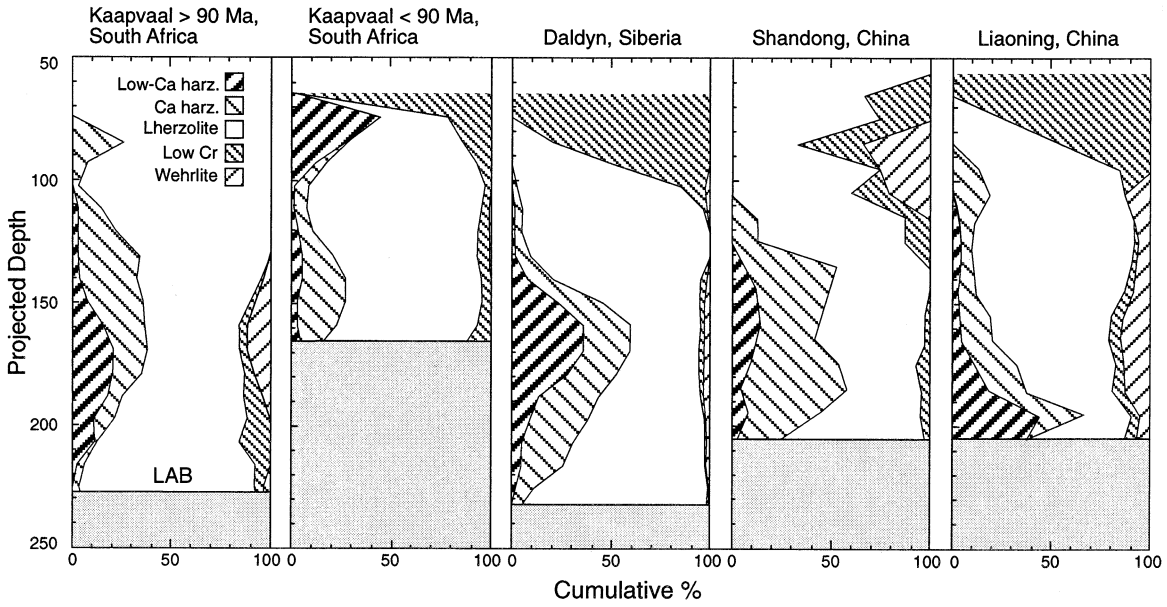


Fig. 2. Lithologic sections through the lithospheric mantle of several Archean cratons, constructed using the compositions and calculated temperatures of garnet xenocrysts ([47,7,14]). The grey shading represents the asthenosphere. Note that for the Kaapvaal craton, the two time slices are shown representing mantle xenoliths sampled by kimberlites intruded before and after 90 Ma.

essentially those expected from a constant mantle heat flow, but variable crustal heat production ([9,11]). In areas of basaltic volcanism, such as eastern Australia and eastern China, xenoliths and xenocrysts in basalts generally record high, strongly convex-upward geotherms, consistent with advective heat transport by magmas and underplating of basaltic magmas in the upper part of the lithospheric mantle ([12]).

### 2.2. Estimation of lithosphere thickness

Once the palaeogeotherm has been estimated from xenolith/xenocryst data or heat-flow modelling, temperature estimates for individual samples can be projected to this palaeogeotherm to determine their depth of origin. This approach has proved especially fruitful for use with xenocryst suites, because statistically meaningful numbers of samples can be gathered for each section, something which often is difficult to achieve with xenoliths alone. By determining the Nickel Temperature ($T_{Ni}$) of individual garnet grains in a heavy-mineral concentrate, and the Zinc Temperature ($T_{Zn}$) of individual chromites, the geochemical information contained in each grain can be placed in stratigraphic context, to map the vertical distribution of rock types and geochemical process signatures ([6,13]).

The resulting lithological/geochemical columns (Fig. 2) provide 1-D maps, equivalent to drill hole logs, through individual lithospheric sections. Griffin and Ryan [13] and Ryan et al. [6] have shown that beneath many volcanic provinces there is a sharply defined maximum depth at which garnets depleted in yttrium (a lithosphere signature) are common (Fig. 3). They have argued that this depth represents the base of the petrologically defined lithosphere, and thus corresponds to the LAB. In most localities worldwide, this petrologically defined LAB corresponds to temperatures of 1250–1300°C [6]. The depth of the LAB mapped in this way varies broadly with tectonic setting, being deepest (250–150 km) beneath Archean terrains (e.g. [7,14]) and shallowest beneath Phanerozoic terrains (Fig. 1), as would be expected from the observed variation in the palaeogeotherms beneath terrains of different age (Fig. 1a). Where high-quality deep seismic data are available, this LAB commonly corre-

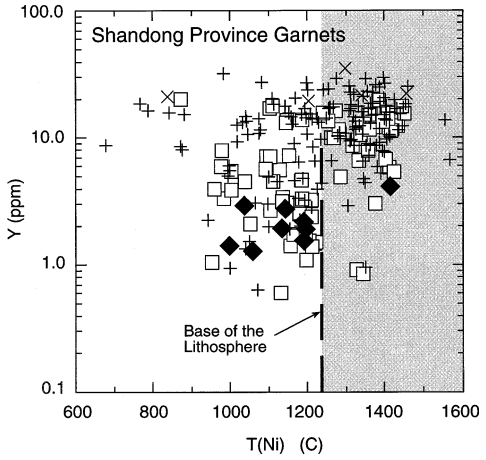


Fig. 3. $Y$–$T_{Ni}$ (Ni temperature; [6]) plot for garnets from kimberlites of Shandong Province, eastern China, showing the LAB defined by the deepest occurrence of $Y$-depleted garnets. After Griffin et al. [47].

sponds to the L (Lehman) discontinuity in cratonic areas (e.g. [1]). Various geophysical and geochemical definitions of the nature of the LAB have been discussed in ([1] and references therein). These different estimates converge at similar depths and may indicate the interdependence of thermal state, rheology and phase relationships in determining the location of this boundary in different sections.

## 3. Secular variation of lithosphere composition

Isotopic studies, especially of the Re–Os system, show that the lithospheric mantle beneath Archean cratons (=2.5 Ga, as defined by the age of the last major tectonothermal event to affect the crust; [15]) is largely Archean in age, while that beneath Proterozoic crust is largely Proterozoic in age ([16–19]). These studies provide a priori evidence that the formation of the crust and the SCLM are linked processes, and suggest that a detailed analysis of the tectonothermal history of a crustal volume provides a basis for estimating the formation age of the underlying SCLM.

Boyd ([20,21]) recognised a fundamental distinction between Archean cratonic SCLM, represented by xenoliths of peridotitic mantle from African and Siberian kimberlites, and Phanerozoic circumcratonic mantle, represented by xenoliths of peridotitic mantle in intraplate basalts and by orogenic lherzolite massifs. Compared to Phanerozoic mantle, the peridotite xenoliths from oncraton kimberlites are not only more depleted on average, but have higher Si/Mg (higher opx/olivine). This distinctive feature is common to both lherzolites and harzburgites, and to rocks of both garnet and spinel facies [22].

Analysis of a large database of xenolith compositions ([23,24]) also demonstrates that Archean xenoliths have lower Ca/Al, Fe/Al and Cr/Al ratios at equivalent mg# than xenoliths from Proterozoic and Phanerozoic regions. Archean SCLM is distinctive in another important respect: subcalcic (clinopyroxene-free) harzburgites are well represented in Archean xenolith and xenocryst suites, but essentially absent in younger ones ([23,24]). These data clearly indicate that the SCLM beneath Archean cratons and younger terranes is compositionally different. A larger dataset, covering a larger geographic range, is provided by geochemical analyses of garnet xenocrysts (disaggregated from peridotitic mantle xenoliths) in volcanic rocks and derived alluvial concentrations. Analysis of >13 000 Cr–pyrope garnet xenocrysts from volcanic rocks worldwide shows a clear correlation of average garnet composition with the tectonothermal age of the crust penetrated by the volcanic rocks [14].

### 3.1. Calculating the composition of lithospheric mantle

If the composition of SCLM varies with tectonothermal age, the interpretation of geophysical data and understanding of tectonic processes requires that we consider differences in the mean composition of the different types of SCLM beneath the major tectonic divisions noted above. The great bulk of the existing analytical data for Archean xenoliths comes from a small area of the Kaapvaal craton in South Africa, and from a single kimberlite pipe in Siberia (Udachnaya); there are very few xenolith data for Proterozoic terranes. However, abundant data from garnet concentrates are available for many of the world's

Table 1
Comparison of mean mantle compositions calculated from garnets, with average compositions of xenolith suites (after Griffin et al. [24])

| | Kaapvaal <90 MA Garnet lherzolite (Calculated from Garnets) | Kaapvaal Lherzolite xenoliths (Median) | Kaapvaal <90 MA Garnet harzburgite (Calculated from Garnets) | Kaapvaal Harzburgite xenoliths (Median) | Vitim Garnet lherzolite (Calculated from Garnets) | Vitim Lherzolite xenoliths (Median) |
|---|---|---|---|---|---|---|
| *Wt%* | | | | | | |
| $SiO_2$ | 46.0 | 46.6 | 45.7 | 45.9 | 44.5 | 44.5 |
| $TiO_2$ | 0.07 | 0.06 | 0.04 | 0.05 | 0.15 | 0.16 |
| $Al_2O_3$ | 1.7 | 1.4 | 0.9 | 1.2 | 3.7 | 4.0 |
| $Cr_2O_3$ | 0.40 | 0.35 | 0.26 | 0.27 | 0.40 | 0.37 |
| FeO | 6.8 | 6.6 | 6.3 | 6.4 | 8.0 | 8.0 |
| MnO | 0.12 | 0.11 | 0.11 | 0.09 | 0.13 | 0.10 |
| MgO | 43.5 | 43.5 | 45.8 | 45.2 | 39.3 | 39.3 |
| CaO | 1.0 | 1.0 | 0.5 | 0.5 | 3.3 | 3.2 |
| $Na_2O$ | 0.12 | 0.10 | 0.06 | 0.09 | 0.26 | 0.32 |
| NiO | 0.27 | 0.28 | 0.30 | 0.27 | 0.25 | 0.25 |

cratonic areas and these expand our picture of SCLM variability.

In xenolith suites, the $Cr_2O_3$ content of garnet correlates well with the $Al_2O_3$ content of the host rock ([23,24]). These suites also show good correlations between the content of $Al_2O_3$ and those of other major and minor elements. Such correlations make it feasible to calculate the bulk composition of a mantle section, given the median $Cr_2O_3$ content of garnet xenocrysts from that section; the technique gives good agreement with the average compositions of xenolith suites, where suitably large data sets are available (Table 1; see other examples in Griffin et al. [24]).

The mean composition of SCLM beneath terranes of Archean, Proterozoic and Phanerozoic tectonothermal age, calculated in this way, shows a secular evolution in all measures of depletion, such as Al, Ca, mg#, and Fe/Al (Table 2). The existing database is not sufficient to establish whether this secular evolution is continuous or discontinuous; for the purposes of this work we adopt the broad divisions recognised by Griffin et al. [25,26], who divide the datasets into Archean (tectonothermal age = 2.5 Ga), Proterozoic (2.5–1.0 Ga) and Phanerozoic ( = 1.0 Ga).

Unmodified Proterozoic SCLM is moderately depleted, and intermediate in composition between Archean and Phanerozoic SCLM. Cenozoic SCLM, exemplified by the Zabargad peridotites of the Red Sea and by garnet peridotite xenoliths from young extensional areas of China, Siberia and Australia, is only mildly depleted relative to Primitive Upper Mantle (PUM: [3,23–25]). SCLM beneath some Phanerozoic terrains, especially in Europe, is more depleted and may represent reworked Proterozoic SCLM (Table 2: preferred values). The correlation of SCLM composition with crustal age is strong evidence that crustal volumes and their underlying lithospheric mantle formed quasi-simultaneously, and that syngenetic crust and mantle can, and in most cases do, remain linked for periods of aeons.

## 4. Calculating the density of SCLM

For each of the mean SCLM compositions defined above (Table 2), we have estimated mean mineral compositions, based on broad correlations between mineral and rock compositions in xenoliths ([23]). These mineral compositions have then been used to calculate the modal compositions of the average Archean, Proterozoic and Phanerozoic SCLM (Table 2). We have approximated the composition of the asthenosphere by the Primitive Mantle composition of McDonough and Sun [26], which is close to the pyrolite com-

Table 2
Calculated mean compositions for Archean, Proterozoic and Phanerozoic SCLM (after Griffin et al. [24]), modes, mineral compositions, and selected calculated ratios and constant values

| | Archean Gnt-calc SCLM | Proterozoic Gnt-calc SCLM | Proterozoic Xenoliths, massifs | Phanerozoic Gnt-calc SCLM | Phanerozoic spinel peridotite (preferred) | Primitive Mantle [26] |
|---|---|---|---|---|---|---|
| *Wt%* | | | | | | |
| $SiO_2$ | 45.7 | 44.7 | 44.6 | 44.5 | 44.4 | 45.0 |
| $TiO_2$ | 0.04 | 0.09 | 0.07 | 0.14 | 0.09 | 0.2 |
| $Al_2O_3$ | 0.99 | 2.1 | 1.9 | 3.5 | 2.6 | 4.5 |
| $Cr_2O_3$ | 0.28 | 0.42 | 0.40 | 0.40 | 0.40 | 0.38 |
| FeO | 6.4 | 7.9 | 7.9 | 8.0 | 8.2 | 8.1 |
| MnO | 0.11 | 0.13 | 0.12 | 0.13 | 0.13 | 0.14 |
| MgO | 45.5 | 42.4 | 42.6 | 39.8 | 41.1 | 37.8 |
| CaO | 0.59 | 1.9 | 1.7 | 3.1 | 2.5 | 3.6 |
| $Na_2O$ | 0.07 | 0.15 | 0.12 | 0.24 | 0.18 | 0.36 |
| NiO | 0.30 | 0.29 | 0.26 | 0.26 | 0.27 | 0.25 |
| *Ratios* | | | | | | |
| mg# | 92.7 | 90.6 | 90.6 | 89.9 | 89.9 | 89.3 |
| Mg/Si | 1.49 | 1.42 | 1.42 | 1.33 | 1.38 | 1.25 |
| Ca/Al | 0.55 | 0.80 | 0.80 | 0.82 | 0.85 | 0.73 |
| Cr/Cr+Al | 0.43 | 0.30 | 0.30 | 0.17 | 0.18 | 0.05 |
| Fe/Al | 4.66 | 2.64 | 2.64 | 1.66 | 2.23 | 1.30 |
| *Modes* | | | | | | |
| ol/opx/cpx/gnt | 69/25/2/4 | 70/15/7/8 | 70/17/6/7 | 60/17/11/12 | 66/17/9/8 | 57/13/12/18 |
| *Mineral compositions* | | | | | | |
| Olivine | $Fo_{93}$ | $Fo_{91}$ | $Fo_{91}$ | $Fo_{90}$ | $Fo_{90}$ | $Fo_{90}$ |
| Orthopyroxene | $En_{93}$ | $En_{91}$ | $En_{91}$ | $En_{90}$ | $En_{90}$ | $En_{90}$ |
| Clinopyroxene[a] | $Di_{70}$ $Hd_{10}$ $Jd_{10}Cc_2En_8$ | $Di_{70}$ $Hd_{10}$ $Jd_{10}Cc_2En_8$ | $Di_{70}$ $Hd_{10}$ $Jd_{10}Cc_2En_8$ | $Di_{70}$ $Hd_{10}$ $Jd_{10}Cc_2En_8$ | $Di_{70}$ $Hd_{10}$ $Jd_{10}Cc_2En_8$ | $Di_{70}$ $Hd_{10}$ $Jd_{10}Cc_2En_8$ |
| Garnet[b] | $Py_{70}Alm_{15}$ $Uv_{15}$ | $Py_{70}Alm_{25}$ $Uv_5$ | $Py_{70}Alm_{25}$ $Uv_5$ | $Py_{70}Alm_{25}$ $Uv_5$ | | $Py_{70}Alm_{25}$ $Uv_5$ |
| *Density* ($Mg/m^3$) | 3.31 | 3.34 | 3.34 | 3.37 | 3.36 | 3.39 |
| *Constants* | | | | | | |
| $a_0 \times 10^{-4}$ | 0.27165 | 0.27014 | – | 0.2697 | 0.27768 | – |
| $a_1 \times 10^{-8}$ | 1.04971 | 1.05945 | – | 1.0192 | 0.95451 | – |
| $a_2$ | −0.15031 | −0.1243 | – | −0.1282 | −0.12404 | – |
| $k$ | 129 | 130 | – | 130 | 128 | 134 |

[a] Di = diopside, Hd = hedenbergite, Jd = jadeite, Cc = cosmochlore, En = enstatite.
[b] Py = pyrope, Alm = almandine, Uv = uvarovite.

position of Ringwood [27]. The assumption that the major-element composition of the modern asthenosphere is only slightly depleted relative to PUM is supported by the common occurrence of Phanerozoic xenoliths with near-PUM compositions, as noted above.

The calculated modes (Table 2) illustrate the increase in modal garnet+clinopyroxene and clinopyroxene/garnet from Archean to Proterozoic to Phanerozoic SCLM, and the relatively small degree of depletion of Phanerozoic SCLM relative to Primitive Mantle compositions. The mean density of each SCLM composition at surface temperature ($T$) and pressure ($P$) has then been calculated by combining the modes and mineral compositions with the end-member mineral densities of Smyth and McCormick [28].

The major controls on density are mg# and the proportion of olivine to clinopyroxene+garnet, and these are the parameters that probably are best constrained in these calculations. A change of 1% ($>1\sigma$) in the mg# of olivine results in a change in density of 0.008 Mg m$^{-3}$. In Archean rocks, a variation of 50% ($1\sigma$; [23]) in the abundance of (cpx+gnt) also produces a variation in density of $\pm 0.008$ Mg m$^{-3}$. These uncertainties will be correlated, because a more iron-rich olivine is likely to be associated with a higher fertility, as expressed in higher (cpx+gnt). The total $1\sigma$ uncertainty in density therefore is on the order of $\pm 0.016$ Mg m$^{-3}$. In the average Proterozoic or Phanerozoic compositions, where the mean (cpx+gnt) is higher, a $\pm 50\%$ variation in (cpx+gnt) has a larger effect, producing a $1\sigma$ uncertainty of 0.02 Mg m$^{-3}$.

Our calculations show a significant increase in mean standard temperature and pressure (STP) density from Archean ($3.31 \pm 0.016$ Mg m$^{-3}$) to Proterozoic ($3.34 \pm 0.02$ Mg m$^{-3}$) to Phanerozoic ($3.36 \pm 0.02$ Mg m$^{-3}$) SCLM. The most depleted Proterozoic SCLM overlaps only the most fertile Archean SCLM at the $1\sigma$ level, while the difference between Proterozoic and Phanerozoic SCLM is much less. The average Archean SCLM is 2.5% less dense than Primitive Mantle (3.39 Mg m$^{-3}$; Table 2) at the same temperature and pressure; for the less-depleted Phanerozoic mantle the difference is about 1%. If Cenozoic lithosphere is assumed to be similar to the more fertile Zabargad peridotites, or the Phanerozoic garnet peridotites (Garnet SCLM of Table 2), the difference drops to about 0.6%.

Jordan [2] used a suite of kimberlite-borne xenoliths to derive a linear relation between normative (at STP) density and mg#, given by $\rho = 5.093–0.019$ mg#. This equation reproduces our derived densities to within 0.01 Mg m$^{-3}$; we are encouraged by the agreement.

Boyd and McAllister [29] used modal estimates and cell-volume data on separated minerals to calculate room-$T$ densities for a strongly depleted Archean garnet lherzolite xenolith (sample PHN1569; $\rho = 3.30 \pm 0.02$ Mg m$^{-3}$) and a high-$T$-sheared peridotite xenolith (sample PHN 1611; density $= 3.39 \pm 0.02$ Mg m$^{-3}$). The density estimate for PHN1569 agrees well with our calculated average for Archean SCLM (Table 1). The density of the sheared xenolith PHN1611 is higher than that of our average Archean lherzolite. However, the garnet and cpx content of PHN1611 has been greatly increased (and its bulk mg# decreased) by high-$T$ melt-related metasomatism shortly prior to its entrainment in the host kimberlite [30]. This 'refertilisation' has produced a bulk composition similar to some 'pyrolite' compositions, and the density of PHN1611 is identical within error of our estimated density for Primitive Mantle, and that of Jordan [31]. Jordan's [31] higher estimated density (3.35 Mg m$^{-3}$) for 'average continental garnet lherzolite' included many high-$T$-sheared lherzolites like PHN1611. However, this class of xenolith appears to be significant only in the deepest parts of the SCLM, and is excluded from the initial analysis given below.

### 4.1. Variation of density with depth

Density variations in the Earth depend on the composition of the mantle section, and are also affected by temperature variations, which in turn affect the elasticity of the minerals; the calculated density at a given depth is a function of the temperature, the bulk thermal expansion coefficient and the bulk compressibility of rock, as determined by the relative proportions of mineral end-members. In this section, we calculate the

variation in density with depth for each average mantle type, assuming a constant composition with depth and using the range of geotherms characteristic of Archean, Proterozoic and Phanerozoic SCLM (Fig. 1).

As noted above, the palaeogeotherms (except for the southeastern Australian 'SEA' geotherm (Fig. 1a)) derived from xenolith and xenocryst data tend to parallel the model conductive geotherms of Pollack and Chapman [8]. In this section of the paper, we therefore have used Pollack and Chapman's conductive model geotherms for calculating $T$-depth relations because these geotherms are easily parameterised.

For each lithosphere type, we assumed a two-layer model with an average crustal thickness of 35 km and a total lithosphere thickness of up to 280 km. For the crust, we assume a constant thermal conductivity of 2.5 W $m^{-1}$ $K^{-1}$. Following Pollack and Chapman [8], we assumed that about 40% of the mean flux arises from surface radiogenic sources, and the rest comes from greater depths. We used this assumption to define an empirical equation relating the reduced heat flow and the mean heat flow at depth, which then defines the distribution of heat production with depth. In our models, we assumed a uniform characteristic depth of heat source distribution, equal to 8 km as defined by Pollack and Chapman [8]. In the case of the mantle, we assumed that there was no heat production, and we used Schatz and Simmons' method [32] to calculate the thermal conductivity of olivine as a function of the temperature and depth. We have parameterised the SEA advective geotherm ([12]) using a spline function. The resulting parameterised geotherms were used to calculate the pressure and temperature-dependent density variations for each mantle type.

To calculate the temperature-dependent density variations, we used the relation:

$$\rho_T = \rho_{20} - (\rho_{20} T \alpha) \quad (1)$$

where $\rho_{20}$ is the density of the section estimated at a room temperature of 20°C (Table 2), $\rho_T$ is the density of the section at a given temperature, and $\alpha$, is the bulk thermal expansion coefficient calculated from the relevant mineral end-members. A polynomial expression of the thermal expansion coefficient is given by [33]:

$$\alpha = a_0 + a_1 T + a_2 T^{-2} \quad (2)$$

where $a_0$, $a_1$ and $a_2$ are constants which are estimated from the mineralogical composition of each mantle type.

The density variations with depth/pressure are also a function of the bulk compressibility of the rocks. A change in pressure will result in a fractional change in the volume of a given mass of material, and this is given by the thermal dilatation or the compressibility $\beta$ of the material, which can be related to the density by the relation:

$$\delta\rho = \rho_T \beta P \quad (3)$$

where $\rho_T$ is the density at a given temperature $T$ and pressure $P$ (GPa).

Table 2 lists the mean composition, the constants of the thermal expansion coefficients ($a_0$, $a_1$, $a_2$) and the bulk moduli ($k = 1/\beta$), calculated from the mineral end-members (Table 2), of the average Archean, Proterozoic, Phanerozoic and Primitive Mantle compositions used in our density calculations.

As temperature changes with depth in the Earth, the competing effects of the compressibility and thermal expansion of the solid phases have significant effects on the density variations with depth [34]. Therefore, we used Eq. 1 to calculate the temperature-dependent density variation with depth, and Eq. 3 to compute the compressibility effect on the density variations with depth. These two effects are then combined to express the temperature and pressure-dependent density variation with depth for Archean, Proterozoic and Phanerozoic mantle sections. In the Phanerozoic section, we have shown the effect on density of the spinel peridotite–garnet peridotite transition at ca 55 km. In the more depleted Proterozoic and Archean sections, the effect of this phase transition is very small (and affects a narrower depth interval of the section as the transition depth decreases with decreasing temperature) and has been ignored; the effect is to give a maximum density

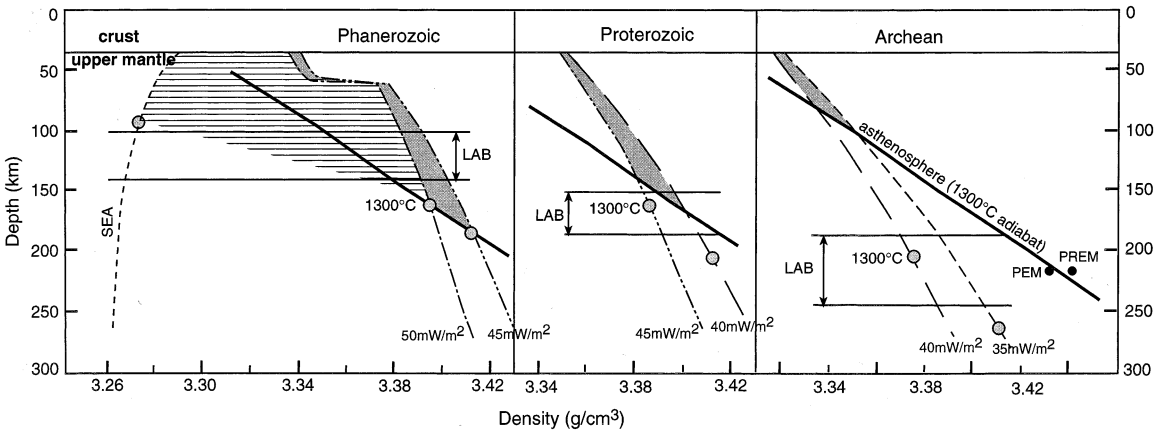


Fig. 4. Plots of density versus depth for lithospheric mantle sections of different age, calculated using the preferred compositions shown in Table 2 and the range of geotherms and LAB depth shown in Fig. 1. SEA, southeastern Australia xenolith-based geotherm, representing advective heat transport in active volcanic areas. This geotherm will decay toward the high conductive geotherms typical of Phanerozoic areas with a time constant of $\approx$10 Ma ([8]). PEM and PREM are the values for the density of the asthenosphere at 220 km depth, based on seismic data and derived from these Earth models (B.L.N. Kennett, pers. commun., 1998). The density of the asthenosphere as a function of depth has been calculated using a Primitive Mantle composition and an adiabat of 0.5°C/km. The shaded areas for each mantle type and age correspond to the sections of the lithosphere that are unstable at any depth relative to the underlying asthenosphere. The rapid increase in density around 55 km on the Phanerozoic curves corresponds to a change in composition from spinel lherzolite (for depths $<$55 km) to garnet lherzolite (for depths $>$55 km). The 1300°C point marking the asthenosphere temperature is shown with grey circles for each geotherm. The horizontal striped area tracks the locus of thermal relaxation from the high advective geotherm.

for these sections. The density of the asthenosphere at the LAB has been calculated using a Primitive Mantle composition (Table 2) (density at 20°C and surface pressure = 3.288 Mg $m^{-3}$). We represent the LAB by an adiabat with a potential temperature of 1300°C, independent of the different thicknesses of the lithospheric column for SCLM of different types. The density of the asthenospheric (Primitive Mantle) composition as a function of depth is shown in Fig. 4 as a solid heavy line. The density of the asthenosphere at 220 km depth, derived from two standard Earth models based on seismic data (PEM and PREM; B.L.N. Kennett, pers. commun., 1998) shows good agreement with our calculated values (Fig. 4).

The results show that the density of typical Archean lithospheric mantle, within a typical range of cratonic geotherms (35–40 mW $m^{-2}$; Fig. 1a, increases with depth at a slower rate than that of the asthenosphere (Fig. 4), becoming less dense than asthenosphere at about 80–100 km. Typical Proterozoic mantle is denser than the asthenosphere at depths shallower than 145–175 km (depending on the geotherm), but buoyant relative to asthenosphere at greater depths (Fig. 4). In areas of active volcanism, where advective heat transport by magmas raises the geotherm (e.g., the SEA geotherm; [12]), Phanerozoic mantle actually decreases in density with depth due to the overriding effects of thermal expansion. Where the geotherm approximates a steady-state conductive model, and within the range typically observed in older, tectonically inactive Phanerozoic terrains, the density of Phanerozoic mantle increases with depth in the shallow spinel lherzolite stability field, rises sharply at the spinel–garnet lherzolite transition (ca 55–65 km) and then rises again with depth in the garnet lherzolite stability field (below ca 55 km). The density increase due to the phase change is about 3%. At depths of 160–185 km in areas with a typical Phanerozoic conductive geotherm, the density of Phanerozoic SCLM approaches that of the asthenosphere; in thinner sections the lithosphere is denser than the subjacent asthenosphere.

To evaluate the stability of different lithospheric sections relative to the asthenosphere, it is use-

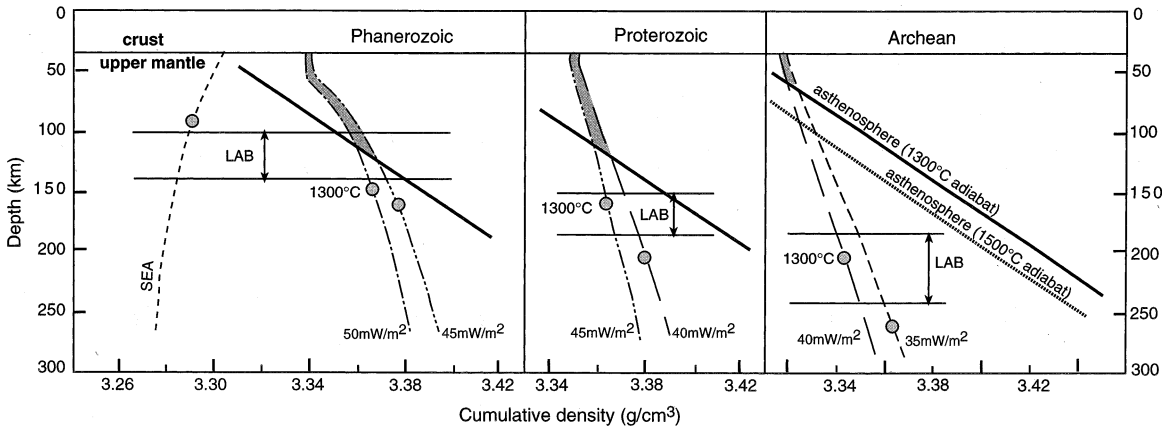


Fig. 5. Plots of cumulative density versus lithosphere thickness for lithospheric mantle sections of different age, calculated using the preferred compositions shown in Table 2 and the range of geotherms and LAB depth shown in Fig. 1. The shaded areas for each mantle type and age correspond to the integrated sections of the lithosphere that are unstable relative to the underlying asthenosphere. The thick line indicating the density of the asthenosphere as a function of depth assumes a Primitive Mantle composition (Table 2) and an adiabat of 0.5°C/km for the LAB. The striped line on the Archean plot shows the density of a hotter asthenosphere (1500°C) calculated with an adiabat of 0.5°C/km. Same abbreviations as in Fig. 4.

ful to calculate the cumulative density of each column as a function of its thickness, and to compare this density with that of a column of asthenospheric mantle whose temperature follows the 1300°C adiabat (Fig. 5). These curves demonstrate that sections of Archean lithospheric mantle thicker than ca 60 km are buoyant relative to the underlying asthenosphere. Typical Archean lithosphere is 150–250 km thick (Fig. 1) and therefore these sections are significantly buoyant; a 200-km section is 2.5% less dense than the asthenosphere at the LAB. A Proterozoic SCLM section thicker than ca 125 km is buoyant relative to the asthenosphere, but less so than Archean lithosphere; typical sections 160 km thick are ca 1% less dense than the asthenosphere at the LAB. Phanerozoic SCLM sections with advective geotherms decrease in density with depth, and are strongly buoyant relative to the asthenosphere. However, older sections that have cooled to steady-state conductive geotherms are buoyant relative to the asthenosphere only if they are more than 110–120 km thick.

Fig. 6 summarises lithospheric density profiles for each SCLM age type and the upper asthenosphere. The geotherm used for each SCLM section is within the typical range shown in Figs. 4 and 5: the asthenosphere thermal state assumes a potential temperature of 1300°C and an adiabat of 0.5°C/km. This figure emphasises the density contrasts between lithospheric sections of different ages and the relationship between the density of each lithospheric section and that of the underlying asthenosphere.

## 5. Discussion

### 5.1. Comparison with other models

Jordan [2] showed that the elevation of the continents, and particularly of the cratonic areas requires a chemical boundary layer beneath the continents that is buoyant relative to oceanic mantle. He also gave a formulation for the condition for marginal stability in a layer with such a lateral variation in density, which gives a minimum value for the compositional density contrast across the layer. One profile that satisfies this condition for Archean lithosphere is the isopycnic curve, in which the density of the lithospheric column at each depth is the same beneath oceans and continents [2]. The negative buoyancy produced by the lower temperature gradient of continental lithosphere is balanced by a positive buoyancy due to a more depleted composition. This formu-

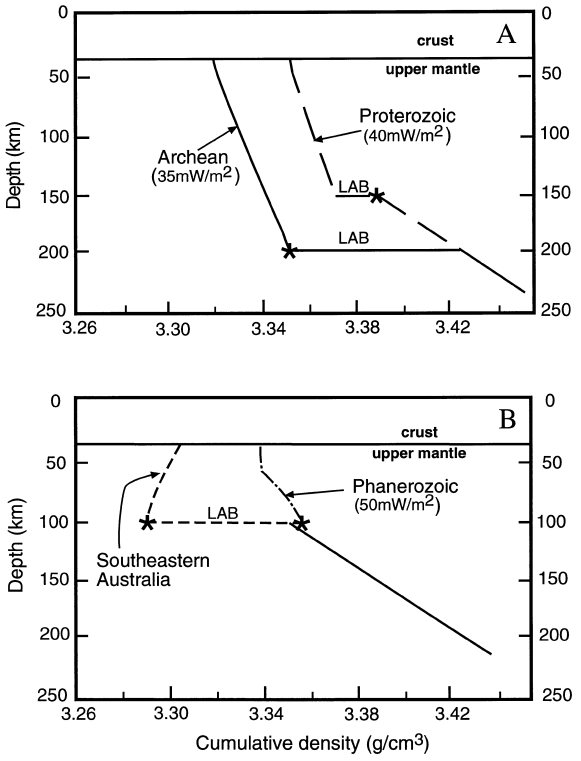


Fig. 6. Density profiles for each lithospheric mantle age type and for the upper asthenosphere: Primitive Mantle composition from Table 2 is used for the asthenosphere composition with an adiabat of 0.5°C/km. The representative average (labelled) geotherm for each lithosphere section is within the typical geotherm range shown in Figs. 3 and 5. The stars show where the geotherms for each lithosphere section cross the LAB. The average LABs taken from Figs. 4 and 5 are 200, 150 and 100 km for the Archean, Proterozoic and Phanerozoic lithosphere, respectively.

lation requires that the normative density (at STP) of the continental section increases with depth. The isopycnic curve, corrected for the effects of $T$ and $P$, would necessarily approximate the density of the asthenosphere as shown on Fig. 5. This represents a minimum buoyancy; a continent with a lithospheric density profile corresponding to the isopycnic curve would have little or no freeboard relative to the oceans.

Jordan [2] used xenolith data to argue that the normative density of the Archean lithosphere increases with depth as required by the isopycnic hypothesis. A more detailed analysis based on the study of garnet xenocrysts in volcanic rocks from cratonic areas worldwide ([35]) confirms a general decrease in mg# with depth, implying that the density of the lower parts of Archean and Proterozoic sections can approach that of Phanerozoic lithosphere. However, this effect is most pronounced in the deeper parts of the lithosphere ($>180$ km depth) and represents a rapid increase in density over a short vertical distance; a similar distribution of density with temperature is seen in the data used by Jordan ([2], Fig. 3).

The cumulative density curves shown in Fig. 5, which assume a constant normative density, probably give the maximum buoyancy contrast to be expected for each type of lithospheric section. The Archean lithosphere approximated in this way shows significant buoyancy for sections with typical Archean lithosphere thicknesses of 180–220 km, while Proterozoic sections with typical thicknesses of 150–180 km are only moderately buoyant, and Phanerozoic sections (100–130 km thick) are neutrally buoyant. The low to moderate buoyancy of Proterozoic and Phanerozoic lithosphere, relative to the asthenospheric mantle, satisfies the minimum requirements for marginal stability in the plate. However, in contrast to the isopycnic situation, the density–depth curves derived here show lithospheric densities greater than that of the asthenosphere at shallow depths, and less than that of the asthenosphere at greater depths. The very low normative densities at shallow depths implied by the isopycnic relation would require Archean-type densities at Moho depths beneath all sections, and there is no evidence in the xenolith record for this except in some Archean sections. The overall buoyancy of Archean sections (Fig. 5) probably is a maximum estimate, if the rapid decrease in mg# at depths of 180–220 km observed by Gaul et al. [35] is a general feature of Archean lithosphere, but even with this caveat, it appears that Archean lithosphere is significantly positively buoyant with respect to the underlying asthenosphere. Is such buoyancy compatible with observation?

Jordan [36] argued that cratons are neutrally buoyant relative to oceanic mantle because they are not observable in the long-wavelength gravity field. Richards and Hager [37] and Forte et al. [38] found that in fact there is a weak association

between geoid perturbations and the continental shields, while Shapiro et al. [39] argued that this difference is not significant at the $2\sigma$ level. However, the wavelengths used (of necessity) in these studies may be too long to recognise the significant buoyancy of Archean domains. The parameterisations have grouped Archean and Proterozoic shield areas, which will tend to combine large areas of neutrally to slightly buoyant Proterozoic shields with smaller areas underlain by more buoyant Archean keels, leading to a small total signal at such long wavelengths. On a smaller (regional) scale, analysis of upward-continued gravity data indicates a significant density deficit beneath Archean cratons, but not beneath the surrounding Proterozoic mobile belts (Poudjom Djomani et al., in prep.).

### 5.2. Can continental lithosphere 'delaminate'?

The cumulative density curves in Fig. 5 provide some constraints on tectonic and geochemical models that invoke the gravity-driven detachment ('delamination') of SCLM and its recycling into the deep mantle. Our results show that a typical section of Archean lithospheric mantle is significantly buoyant relative to the asthenosphere. Lowering the geotherm below the 35 mW/m$^2$ conductive model could increase the density of the column, but even if the geotherm were greatly depressed, such a section of Archean SCLM is unlikely to become negatively buoyant if it is thicker than 100 km. Tectonic stacking, often invoked as a mechanism for delamination, will simply increase the buoyancy of the Archean SCLM section relative to the asthenosphere, as the density of the asthenosphere at the depressed LAB increases faster than that of the thickened lithosphere, assuming constant composition. This type of lithospheric mantle therefore cannot be delaminated through gravitational forces alone.

The compositional buoyancy of Archean SCLM also acts to stabilise the TBL against convective disruption by reducing the stress, which leads in turn to a reduction in viscosity and an increase in strength. Such compositional buoyancy appears to be required by flow models that invoke activation energies less than those required for the flow of olivine [40]. Finally, the refractory nature and low heat production of the Archean lithosphere reduces the probability of its being weakened by partial melting, even when subjected to relatively large temperature perturbations. The combined effects of their highly depleted compositions on buoyancy, strength and resistance to melting provide a simple explanation for the thickness and apparent long-term stability of Archean lithospheric roots.

Proterozoic SCLM, while denser than Archean SCLM at the same temperature because of its less depleted composition, also typically has somewhat higher geotherms (Fig. 1). Any Proterozoic section more than about 150–180 km thick is moderately buoyant (Fig. 5), consistent with the observed preservation of lithosphere with Proterozoic Re–Os ages beneath Proterozoic cratons (e.g. [16–19]) and beneath some areas where Phanerozoic tectonic (but not magmatic) activity has reworked Proterozoic crust, such as the Caledonides of western Norway ([41]) and parts of western Europe ([23]). Because the density contrast between asthenosphere and Proterozoic SCLM at the LAB is less than for Archean SCLM, it is possible that a decrease in the geotherm below those modelled here could destabilise a section as thick as 150 km.

Phanerozoic terranes have a wide range of geotherms (Fig. 1). With the high advective geotherms, typical of areas of active or recent basaltic volcanism (e.g. [12,42]), Phanerozoic SCLM is extremely buoyant. Some Phanerozoic SCLM sections may sustain relatively high conductive geotherms because they have high internal heat production. However, with lower geotherms observed in older Phanerozoic areas (45–50 mW/m$^2$ conductive models; Figs. 1, 4 and 5), a section of Phanerozoic SCLM thinner than about 110 km is denser than the asthenosphere at the LAB, and hence is gravitationally unstable. This is a minimum estimate: if the denser Cenozoic lithospheric mantle found as garnet peridotites in some regions (e.g. eastern China; [3]) is considered, sections up to about 150 km thick are unstable even on the higher conductive geotherms characteristic of many Phanerozoic terranes.

Lithosphere delamination, accompanied by the

upwelling of the asthenosphere to shallow depths, is widely invoked to explain tectonic uplift and crustal magmatism and metamorphism. The data presented here suggest that this mechanism is unlikely to have been relevant during the growth of Archean cratons, unless the lithospheric roots of these cratons formed after the major magmatic/metamorphic episodes. However, available Re–Os data suggest that such roots are at least as old as the overlying crust ([16] and references therein).

On the other hand, the density–depth systematics of Phanerozoic SCLM suggest that such delamination is highly likely as a result of cooling following crustal formation.

### 5.3. 'Lithosphere erosion' – mechanisms and effects

The data presented here suggest that tectonic or magmatic events that lead to the replacement of old SCLM by younger material will cause changes in the density and geothermal profile of the lithospheric column, with major effects at the surface. These effects will include regional uplift due to the lower density of material on an elevated geotherm [43], followed by subsidence as the elevated geotherm relaxes [44] and the overall density of the section increases due to the replacement of older buoyant mantle with younger, denser mantle.

Several studies have documented situations in which thick, depleted (Archean) lithospheric mantle has been wholly or partially removed and replaced by thinner, hotter and more fertile SCLM. Eggler et al. [45] showed that beneath the Wyoming craton, an original Archean lithosphere about 200 km thick, with a low conductive geotherm, has been largely replaced by fertile Cenozoic SCLM with a thickness of about 120 km. In the Kaapvaal Craton, Brown et al. [46] used fission track dating and xenolithic material from kimberlites of different ages to show that the removal of ca 40 km of old, depleted lithospheric mantle and its replacement by hotter and chemically recharged (metasomatised) lithosphere around 90 Ma ago, is correlated with significant uplift and erosion of the craton. In the eastern Sino–Korean craton, China, the removal of about 100 km of Archean lithosphere during the late Mesozoic was accompanied by uplift, basin formation and widespread magmatism [47].

If, as argued above, Archean SCLM cannot be 'delaminated' and is too refractory to be melted significantly, how does such lithosphere replacement occur? A detailed discussion of possible scenarios is outside the scope of this paper. However, at least one mechanism is suggested by geological and geophysical studies of the Sino–Korean craton. Detailed seismic tomography of part of the eastern Sino–Korean craton, an area of very high heat flow, shows a lithospheric mantle made up of vertically and laterally extensive blocks of high-velocity (probably Archean) mantle embedded in a matrix of lower-velocity (presumably Cenozoic) mantle [48]. Yuan [48] suggests that this heterogeneity reflects the disruption of the Archean lithosphere due to rifting processes that allowed upwelling of young fertile mantle along breaks in the Archean root. This mechanism has resulted in mechanical dispersal, heating and 'dilution' of the Archean root, rather than its removal. We suggest that the prolongation of this process would involve heating and metasomatism of the relict Archean blocks by asthenospheric material, leading to a progressive increase in normative density and decrease in their buoyancy and viscosity, to the point where they would be difficult to distinguish from young lithosphere, except possibly by isotopic techniques.

### 5.4. Implications for lithosphere generation processes

The material of Archean SCLM is so buoyant relative to asthenosphere that even relatively small volumes would rise and accumulate, especially if they were generated in high-temperature events [49] so that their density would be lower than modelled in Figs. 4 and 5. Fig. 5 shows the effect of a hotter asthenosphere in the Archean, modelled as an adiabat with a potential temperature of 1500°C. Even in this situation, Archean lithosphere thicker than ca 75 km would be significantly buoyant. This buoyancy offers a mechanism for generating Archean protocontinents from the depleted residues of small-scale events. Indeed, it would be difficult not to accumulate

such material, and the current lack of Re–Os depletion ages greater than ca 3.5 Ga for mantle materials may imply that these lithosphere-forming processes did not begin earlier.

The relatively low density of a hotter asthenosphere could have led to the preferential preservation of only the least dense lithosphere sections, thus exaggerating the apparent contrast in normative density between Archean and younger lithosphere. However, if this density-sorting mechanism was the primary cause, we would expect to find Archean-type material in younger lithosphere sections, and this has not been identified to date ([24]). Thus even if only the most buoyant parts of the Archean lithosphere have survived, the differences between Archean and younger SCLM argue for a secular change in the processes that have generated SCLM through time. Discussions of the nature of these processes are given elsewhere [25,26,49].

Proterozoic lithospheric sections are typically 150–180 km thick, but are only gravitationally stable if they are 130 km thick. These thick sections would have to have accumulated either rapidly, or at high enough temperatures to remain buoyant until they have thickened to the point where thermal relaxation would not make them unstable. This accumulation would be assisted by secular cooling of the Earth, as the cooler asthenosphere became more dense. The processes that produced these relatively thick stable roots appear to be largely confined Archean and Proterozoic time, though present-day analogues may exist under regions such as the Sierra Nevada of California.

A section of Phanerozoic SCLM cooling from a high advective geotherm (such as the SEA geotherm (Figs. 4 and 5) toward a typical high conductive geotherm undergoes a dramatic change in density ($>2\%$ for a section 100 km deep). While this section is very buoyant on the high advective geotherm it is gravitationally unstable and subject to delamination (Rayleigh–Taylor instability; [50] and references therein) on lower geotherms. The removal of such a section, and its replacement by upwelling asthenospheric material, would produce a new advective geotherm, starting the cycle over again. This instability may be a common feature of Phanerozoic orogenic belts, and could explain the apparent scarcity of oceanic or island–arc depleted mantle components in xenolith suites from young mobile belts such as eastern China and eastern Australia, as documented by Griffin et al. [23,24].

## 6. Conclusions

Differences in SCLM composition and geotherms between Archean, Proterozoic and Phanerozoic regions result in marked, age-related differences in mean lithospheric density and in the density–depth relationship within the SCLM.

Archean SCLM sections (depth to base of lithosphere 180–240 km) are significantly buoyant relative to asthenosphere under any reasonable geological scenario, and this buoyancy reduces both stress and viscosity. Therefore Archean SCLM cannot be delaminated by gravitational processes alone, and will tend to be preserved. Tectonic processes such as rifting may allow its disruption and replacement by upwelling, more fertile asthenospheric (or plume) material.

Proterozoic SCLM is less depleted and therefore denser (at the same T) than Archean SCLM. Thin Proterozoic SCLM (less than about 120 km thick) is denser than asthenosphere and would be gravitationally unstable. However, Proterozoic lithospheric sections are typically 150–180 km thick; such SCLM columns are moderately buoyant and, like Archean SCLM, are unlikely to be delaminated.

Phanerozoic lithospheric sections are commonly less than about 100 km thick. These sections are stable under the elevated geotherms associated with volcanic activity, but gravitationally unstable once they have cooled to typical steady-state conductive geotherms. This instability suggests that lithospheric delamination may be a common feature of the history of Phanerozoic mobile belts. Replacement of such a section by upwelling asthenospheric material will start another cycle of cooling, instability and delamination. This process may explain the common occurrence of highly fertile SCLM beneath Phanerozoic mobile belts, where we might instead

expect to find depleted oceanic and arc-related peridotites.

## Acknowledgements

The concepts discussed here owe much to discussions with many colleagues, including Joe Boyd, Rod Brown, Geoff Davies, Buddy Doyle, Kevin Kivi, Lev Natapov, Norm Pearson, Chris Ryan, Yuan Xuecheng and Ming Zhang. We thank Brian Kennett for providing his independent estimates of asthenosphere density at 220 km and A. Lenardic for helpful comments on an earlier version of this manuscript. Comments by I. Artemieva and an anonymous reviewer have clarified issues in the manuscript. Funding for this work has come from several sources, including ARC Large Grants (S.Y.O'R. and W.L.G.), Macquarie University Industry Collaborative Grants, MURG (Y.H.P.D., S.Y.O'R. and W.L.G.), AusAID grants and the mineral exploration industry. This is contribution no 228 from the ARC National Key Centre for Geochemical Evolution and Metallogeny of Continents (www.es.mq.edu.au/gemoc/).*[AC]*

## References

[1] S.Y. O'Reilly, W.L. Griffin, 4-D lithospheric mapping: a review of the methodology with examples, Tectonophysics 262 (1996) 3–18.

[2] T.H. Jordan, Structure and formation of the continental tectosphere, J. Petrol. Special lithosphere issue (1988) 11–37.

[3] X. Xu, S.Y. O'Reilly, W.L. Griffin, X. Zhou, X. Huang, The nature of the Cenozoic lithosphere at Nushan, eastern China, in: M. Flower, S.L. Chun, C.H. Lo, T.Y. Lee (Eds.), Mantle Dynamics and Plate Interactions in East Asia, Geodynamics Series 27, Am. Geophys. Union, Washington, DC, 1998, pp. 167–196.

[4] D. Smith, Temperatures and pressures of mineral equilibration in peridotite xenoliths: review, discussion and implications, in: Y. Fei, C.M. Bertka, B.O. Mysen (Eds.), Mantle Petrology: Field Observations and High-pressure Experimentation: A Tribute to Francis R. (Joe) Boyd, Geochemical Society Special Publication #6, The Geochemical Society, Houston, TX, 1999, pp. 171–188.

[5] A.A. Finnerty, F.R. Boyd, Thermobarometry for garnet peridotite xenoliths: a basis for mantle stratigraphy, in: P.H. Nixon (Ed.), Mantle Xenoliths, John Wiley and Sons, New York, 1987, pp. 381–402.

[6] R.G. Ryan, W.L. Griffin, N.J. Pearson, Garnet Geotherms: a technique for derivation of P–T data from Cr–pyrope garnets, J. Geophys. Res. 101 (1996) 5611–5625.

[7] W.L. Griffin, B.J. Doyle, C.G. Ryan, N.J. Pearson, S.Y. O'Reilly, R.M. Davies, K. Kivi, E. Van Achterbergh, L.M. Natapov, Layered mantle lithosphere in the Lac de Gras area, Slave Craton: composition, structure and origin, J. Petrol. 40 (1999) 705–727.

[8] H.N. Pollack, D.S. Chapman, On the regional variation of heat flow, geotherms and lithosphere thickness, Tectonophysics 38 (1977) 279–296.

[9] P. Morgan, The thermal structure and thermal evolution of the continental lithosphere, Phys. Chem. Earth 15 (1984) 107–193.

[10] R.L. Rudnick, W.F. McDonough, R.J. O'Connell, Thermal structure, thickness and composition of continental lithosphere, Chem. Geol. 145 (1998) 395–411.

[11] C. Jaupart, J.C. Mareschal, The thermal structure and thickness of continental roots, Lithos 48 (1999) 93–114.

[12] S.Y. O'Reilly, W.L. Griffin, A xenolith-derived geotherm for southeastern Australia and its geophysical implications, Tectonophysics 111 (1985) 41–63.

[13] W.L. Griffin, C.G. Ryan, Trace elements in indicator minerals: Area selection and target evolution in diamond exploration, J. Geochem. Explor. 53 (1995) 311–337.

[14] W.L. Griffin, F.V. Kaminsky, C.G. Ryan, S.Y. O'Reilly, L.M. Natapov, I.P. Ilupin, The Siberian Lithosphere Traverse Mantle terranes and the assembly of the Siberian craton, Tectonophysics 310 (1999) 1–35.

[15] A.J.A. Janse, Is Clifford's rule still valid? Affirmative examples from around the world, in: H.O.A. Meyer, O. Leonardos (Eds.), Diamonds: Characterization, Genesis and Exploration, CPRM Spec. Publi. 1A/93, Dept. National da Prod. Mineral., Brazilia, 1994, pp. 215–235.

[16] R. Carlson, D.G. Pearson, F.R. Boyd, S.B. Shirey, G. Irvine, A.H. Menzies, J.J. Gurney, Re–Os systematics of lithospheric peridotites: Implications for lithosphere formation and preservation, vol. 1, Proc. 7th Int. Kimb. Conf., 1999, pp. 99–108.

[17] J.S. McBride, D.D. Lambert, A. Greig, I.A. Nicholls, Multistage evolution of Australian subcontinental mantle Re–Os isotopic constraints from Victorian mantle xenoliths, Geology 24 (1996) 631–634.

[18] M.R. Handler, V.C. Bennett, T.M. Esat, The persistence of off-craton lithospheric mantle: Os isotopic systematics of variably metasomatised southeast Australian xenolith, Earth Planet. Sci. Lett. 151 (1997) 61–75.

[19] B.G. Hoal, K.E.O. Hoal, F.R. Boyd, D.G. Pearson, Age constraints on crustal and mantle lithosphere beneath the Gibeon kimberlite field, Namibia, S. Afr. Tydskr. Geol. 98 (1995) 112–118.

[20] F.R. Boyd, Composition and distinction between oceanic and cratonic lithosphere, Earth Planet. Sci. Lett. 96 (1989) 15–26.

[21] F.R. Boyd, Origin of peridotite xenoliths: major element considerations, in: G. Ranalli et al. (Eds.), High Pressure and High Temperature Research on Lithosphere and Mantle Materials, University of Siena, 1997.
[22] F.R. Boyd, N.P. Pokhilenko, D.G. Pearson, S.A. Mertzman, N.V. Sobolev, L.W. Finger, Composition of the Siberian cratonic mantle: evidence from Udachnaya peridotite xenoliths, Contrib. Mineral. Petrol. 128 (1997) 228–246.
[23] W.L. Griffin, S.Y. O'Reilly, C.G. Ryan, O. Gaul, D. Ionov, Secular variation in the composition of subcontinental lithospheric mantle, in: J. Braun et al. (Eds.), Structure and Evolution of the Australian Continent, Geodynamics Series, Am. Geophys. Union, vol. 26, 1998, pp. 1–25.
[24] W.L. Griffin, S.Y. O'Reilly, C.G. Ryan, The composition and origin of subcontinental lithospheric mantle, in: Y. Fei, C.M. Bertka, B.O. Mysen (Eds.), Mantle Petrology: Field Observations and High-pressure Experimentation: A Tribute to Francis R. (Joe) Boyd, Geochemical Society Special Publication #6, The Geochemical Society, Houston, TX, 1999, pp. 13–45.
[25] D.A. Ionov, I.V. Ashchepkov, H.-G. Stosch, G. Witt-Eickschen, H.A. Seck, Garnet peridotite xenoliths from the Vitim volcanic field, Baikal region: the nature of the garnet–spinel transition zone in the continental mantle, J. Petrol. 34 (1993) 1141–1175.
[26] W.F. McDonough, S. Sun, The composition of the Earth, Chem. Geol. 120 (1995) 223–253.
[27] A.E. Ringwood, The chemical composition and origin of the Earth, in: P.M. Hurley (Ed.), Advances in Earth Science, MIT Press, Cambridge, MA, 1996, pp. 287–356.
[28] J.R. Smyth, T.C. McCormick, Crystallographic data for minerals, in: T.J. Ahrens (Ed.), Mineral Physics and Crystallography: A Handbook of Physical Constants, Am. Geophys. Union, Washington, DC, 1995, pp. 1–17.
[29] F.R. Boyd, R.H. McAllister, Densities of fertile and sterile garnet peridotites, Geophys. Res. Lett. 3 (1976) 509–512.
[30] D. Smith, W.L. Griffin, C.G. Ryan, Compositional evolution of high-temperature sheared lherzolite PHN1611, Geochim. Cosmochim. Acta 57 (1993) 605–613.
[31] T.H. Jordan, Mineralogies, densities and seismic velocities of garnet lherzolites and their geophysical implications, in: F.R. Boyd, H.O.A. Meyer (Eds.), The Mantle Sample: Inclusions in Kimberlites and Other Volcanics, Am. Geophys. Union, Washington, DC, 1979, pp. 1–14.
[32] J.F. Schatz, G. Simmons, Thermal conductivity of Earth materials at high temperatures, J. Geophys. Res. 77 (1972) 6966–6983.
[33] Y. Fei, Thermal expansion, in: T.J. Ahrens (Ed.), Mineral Physics and Crystallography: A Handbook of Physical Constants, Am. Geophys. Union, Washington, DC, 1995, pp. 29–44.
[34] F. Cella, A. Rapolla, Density changes in upwelling mantle, Phys. Earth Planet. Int. 103 (1997) 63–84.
[35] O.F. Gaul, W.L. Griffin, S.Y. O'Reilly, N.J. Pearson, Mapping olivine composition in the lithospheric mantle, Earth Planet. Sci. Lett. 182 (2000) 223–235.
[36] T.H. Jordan, The continental tectosphere, Rev. Geophys. Space Phys. 13 (1975) 1–12.
[37] M.A. Richards, B.H. Hager, The Earth's geoid and the large-scale structure of mantle convection, in: S.K. Runcorn (Ed.), The Physics of Planets, Wiley, New York, 1988, pp. 247–272.
[38] A.M. Forte, A.M. Dziewonski, R.J. O'Connell, Continent–Ocean chemical heterogeneity in the mantle based on seismic tomography, Science 268 (1995) 386–388.
[39] S.S. Shapiro, B.H. Hager, T.H. Jordan, The continental tectosphere and the Earth's long-wavelength gravity field, Lithos 48 (1999) 135–152.
[40] S.S. Shapiro, B.H. Hager, T.H. Jordan, Stability and dynamics of the continental tectosphere, Lithos 48 (1999) 115–133.
[41] B. Jamtveit, D.A. Carswell, E.W. Mearns, Chronology of the high-pressure metamorphism of Norwegian garnet peridotites/pyroxenites, J. Metamorph. Geol. 9 (1991) 125–139.
[42] A.P. Jones, J.V. Smith, J.B. Dawson, E.C. Hansen, Metamorphism, partial melting and K metasomatism of garnet–scapolite–kyanite granulite xenoliths from Lashaine, Tanzanian J. Geol. 91 (1982) 143–165.
[43] P. Morgan, Constraints on rift thermal processes from heat flow and uplift, Tectonophysics 94 (1983) 277–298.
[44] D.P. McKenzie, Some remarks on the development of sedimentary basins, Earth Planet. Sci. Lett. 40 (1978) 25–32.
[45] D.H. Eggler, J.K. Meen, R. Welt, F.O. Dudas, K.P. Furlong, M.E. McCallum, R.W. Carlson, Tectonomagmatism of the Wyoming Province, Colo. Sch. Mines Q. 83 (1988) 25–40.
[46] R.W. Brown, K. Gallagher, W.L. Griffin, C.G. Ryan, M.C.J. De Wit, D.X. Belton, R. Harman, Kimberlites, accelerated erosion and evolution of the lithospheric mantle beneath the Kaapvaal craton during the mid-Cretaceous, Ext. Abst. 7th Int. Kimb. Conf., 1999, pp. 105–107.
[47] W.L. Griffin, A. Zhang, S.Y. O'Reilly, C.G. Ryan, Phanerozoic evolution of the lithosphere beneath the Sino–Korean Craton, in: M. Flower et al. (Eds.), Mantle Dynamics and Plate Interactions in East Asia, Geodynamics Series, vol. 27, Am. Geophys. Union, Washington, DC, 1998, pp. 107–126.
[48] X. Yuan, Velocity structure of the Qinling lithosphere and mushroom cloud model, Sci. China Ser. D 39 (1996) 235–244.
[49] C. Herzberg, Formation of cratonic mantle as plume residues and cumulates, in: Y.Fei, C.M. Bertka and B.O. Mysen (Eds.), Mantle Petrology: Field Observations and High-pressure Experimentation: A Tribute to Francis R. (Joe) Boyd, Geochemical Society Special Publication #6, The Geochemical Society, Houston, TX, 1999, pp. 241–258.
[50] G.A. Houseman, P. Molnar, Gravitational (Rayleigh–Taylor) instability of a layer with non-linear viscosity and convective thinning of continental lithosphere, Geophys. J. Int. 128 (1997) 125–150.